

Dimensional crossover in ultrathin buried conducting SrVO₃ layers

Q.-R. Li

*CRISMAT, CNRS UMR6508, ENSICAEN, Normandie Université, 14050 Caen Cedex 4, France
and Institut für Materialwissenschaft, Technische Universität Darmstadt, 64287 Darmstadt, Germany*

M. Major, M. Baghaie Yazdi, and W. Donner

Institut für Materialwissenschaft, Technische Universität Darmstadt, 64287 Darmstadt, Germany

V. H. Dao, B. Mercey, and U. Lüders*

CRISMAT, CNRS UMR6508, ENSICAEN, Normandie Université, 14050 Caen Cedex 4, France

(Received 13 May 2013; revised manuscript received 19 December 2014; published 15 January 2015)

The structure and resistive properties of buried SrVO₃ layers between two insulating LaVO₃ layers are investigated by varying the thickness of the SrVO₃ layers between 3 and 35 monolayers. The thickest SrVO₃ layer shows a bulklike metallic behavior, while in the thinnest SrVO₃ layer, a weak localization regime is observed below 100 K manifesting a logarithmic temperature dependence. Angular-dependent magnetoresistance measurements indicate a cylindric shape of the Fermi surface, and therefore a two-dimensional transport in the thinnest buried SrVO₃ layer. The modification of the charge carrier properties by the reduced thickness of the SrVO₃ layer are furthermore underlined by the appearance of a relatively strong positive magnetoresistance under a magnetic field perpendicular to the sample surface. The present study therefore highlights a way to synthesize oxide electrodes with reduced dimension for future oxide electronics application.

DOI: [10.1103/PhysRevB.91.035420](https://doi.org/10.1103/PhysRevB.91.035420)

PACS number(s): 73.61.-r, 81.15.-z, 71.27.+a

I. INTRODUCTION

Different systems of two-dimensional electron gases have been under intense investigation for some decades now, due to their importance in present-day electronics and the interesting physics involved in the theoretical description (for a review, see Refs. [1–3]) of the experimental results (for a review, see Ref. [4]). For the experimental studies, typically semiconductor systems are used as they can be synthesized with an extremely high quality and purity, and the charge carrier density can be varied down to very dilute electronic systems in this kind of materials. Most systems can then be described on the basis of weak disorder and low electronic correlations. But little is known of what happens, if the electronic correlations in these two-dimensional systems become very high, as exemplified in the ongoing debate on the origin of high-temperature superconductivity in cuprates.

Apart from the two-dimensional character of the charge carriers, which is a critical ingredient for superconductivity, the characteristics of the cuprates are thought to be those of the complex oxide conductors: a high density of charge carriers with strong electronic correlations. In these other oxide conductors—as, for example, LaNiO₃, SrVO₃, or the manganites—the *d* orbital character of the bands manifests itself in unique features such as fully spin-polarized charge carriers [5,6] or giant magnetoresistance [7]. The high density of the charge carriers and the strong correlations lead in most of these conductors to Mott physics, indicated by Fermi liquid behavior, and eventually a metal-to-insulator transition (MIT) to a Mott insulating state.

However, there are few studies on the electronic properties of two-dimensional systems of these materials. In contrast to

the more investigated two-dimensional (2D) electron gases in semiconductors, the correlations in these oxides give rise to a two-dimensional electron liquid. Within the Mott physics, a reduced bandwidth due to the reduction of dimensionality favors a Mott insulating state. Observations in ultrathin films seem to confirm this prediction: Yoshimatsu *et al.* [8,9] reported that for a single ultrathin film of SrVO₃ (SVO) on SrTiO₃ (STO) substrate, a dimensionality induced MIT occurs at two to three monolayers (ML) of SVO, while beyond 6 ML the bulk metallic state is recovered; more recently, for the same material on (LaAlO₃)_{0.3}(Sr₂AlTaO₆)_{0.7} (LSAT) substrate, Gu *et al.* [10] reported a much thicker crossover thickness (≈ 17 ML) and the presence of a pseudogap, which was ascribed to local metallic states in a globally insulating region. Similar conclusions have been reached by Scherwitzl *et al.* [11] for single ultrathin films of LaNiO₃ (LNO), where the critical thickness distinguishing the insulating and metallic behavior is about 5 ML and a 2D variable range hopping (VRH) can be applied to describe the insulating behavior below room temperature. These reports of an insulating state for the two-dimensional regime support the interpretation that the electronic correlations in two-dimensional oxide conductors are enhanced in such a way, that conduction is suppressed in reduced dimensions. One should, however, notice that typical defects such as oxygen vacancies or lattice deformation due to the strain were not taken into account in these studies, although they may have a more pronounced effect in ultrathin films of only some ML. Also, chemical [12] or structural disorder induced by oxygen vacancies [13] may play a role in the MIT.

On the other hand, 2D electron gases (2DEG) were observed in less correlated oxide systems, such as δ -doped STO [14] and the interface between insulating complex oxides [15]. Jang *et al.* [16] reported that a conducting 2DEG can be obtained by inserting a single atomic layer of a rare-earth oxide using La, Pr, or Nd. They concluded that the strong correlations

*Corresponding author: ulrike.luders@ensicaen.fr

in the 2DEG at the oxide interfaces are due to the electronic transport properties of the inserted rare-earth oxide layers and also the structure and electronic modifications generated in nearby layers. However, the complexity due to the combination of atomic-scale structural and chemical variations prevented them from quantitatively analyzing the experimental data. 2DEG is also observed at the interfaces between insulating complex oxides, for example, the ones between LaTiO_3 [17], LaVO_3 , and SrTiO_3 [18] heterostructures, where the 2DEG is limited around the LaO/TiO_2 interface.

Thus, a two-dimensional conducting state is possible in these latter structures, in contrast to the free surface ultrathin films of SVO and LNO cited before. Two major differences can be identified between these two classes of systems. First, the location of the 2D correlated region is near the surface of the film in one case, while it is buried between structurally compatible insulators in the other case. Second, the STO-based systems do not display signs of correlations as strong as in the materials used for the free surface studies, i.e., LNO and SVO. Therefore, the question arises whether the lack of a bidimensional conducting state in the single film systems of SVO and LNO is a result of the free surface or the peculiarly strong electronic correlations.

It is important to answer this question regarding the understanding of oxide conductors: If the reduction of dimensionality inevitably leads to a Mott insulating phase of strongly correlated charge carriers, the Mott physics are predominant in these systems. If, on the other hand, a two-dimensional conducting state can be reached by burying the conducting zone, the physics of quasiparticles in two dimensions may apply and the theory of the 2DEG could be extended to 2D electron liquids. Apart from this fundamental aspect, a more applicative question would be answered: Is it possible to engineer electrodes which combine both the advantages of 2DEG in semiconductors—i.e., the charge carrier density control by an applied gate voltage—and the features of strongly correlated systems, i.e., for example, a spin-dependent electronic conduction?

Considering all these previous studies, the motivation of the present work is to investigate the conduction state of buried ultrathin SVO layers. This oxide is a correlated $3d^1$ metal oxide with a cubic symmetry and a typical T^2 -dependent resistivity of a Fermi liquid [8,19]. As mentioned earlier, free surface ultrathin samples of this material exhibit a MIT at a thickness of around 3 ML on STO [8,9]. So, studying SVO layers of a comparable thickness buried between insulating layers may therefore allow one to single out the effect leading to the absence of dimensional MIT in the STO-based systems. For the insulating burying material, we choose LaVO_3 (LVO) due to the small lattice mismatch and the absence of interdiffusion down to the limit of some ML [20,21].

We have synthesized trilayer LVO/SVO/LVO on STO(001) substrates with the SVO thickness varying between 3 and 35 ML and investigated their structural and transport characteristics. A thick bottom layer of LVO has been introduced here for separating the SVO layer from the substrate/film interface: STO is known for an easily generated conducting surface or interface with other perovskite oxides, including LVO [18,22]. The top layer of LVO is the burying insulating layer. With the present study, we show that in the buried structures, a

conducting character of the SVO film can be maintained down to 3 ML of SVO and two-dimensional transport behavior can be identified for the thinnest buried SVO layer. Additionally, an unusually strong positive magnetoresistance indicates a conduction state with emergent properties, which are not observed in bulk SVO.

II. EXPERIMENTS

The samples discussed in this paper are prepared by pulsed laser deposition (PLD) on STO(001)-oriented substrates at a substrate temperature of 700°C and chamber pressure of 10^{-5} Torr. The deposition is done from LaVO_4 and $\text{Sr}_2\text{V}_2\text{O}_7$ targets, using the reductive power of ablation in vacuum conditions. A KrF excimer laser was used with a wavelength of 248 nm and pulse rate = 3 Hz. The target-substrate distance was 85 mm in order to achieve low growth rates in the order of $0.2 \text{ \AA}/\text{pulse}$ for LVO and $0.4 \text{ \AA}/\text{pulse}$ for SVO. A single SVO layer grown directly on STO was used as a reference layer to confirm the bulk properties of thick SVO. For the trilayer samples LVO/SVO/LVO, the LVO thickness was fixed to be around 25 nm for each layer. The structural properties and the thickness of the samples were characterized by x-ray diffraction (XRD) using a Seifert 3000P diffractometer ($\text{Cu } K\alpha 1$ with $\lambda = 1.5406 \text{ \AA}$).

The transport properties were measured with the four-point method in a Physical Properties Measurement System (PPMS) by Quantum Design. The magnetic field for the magnetoresistance measurements was applied perpendicular to the film plane, while the angular-dependent magnetoresistance measurements were carried out turning the sample in the applied magnetic field around an in-plane axis. In order to contact the buried SVO layer, deep contacts through the LVO top layer were fabricated by photolithography and ion-beam etching. Four aligned contact holes were opened in the LVO top layer, and filled with silver, resulting in $500 \times 500 \mu\text{m}^2$ square contacts on the buried SVO layer separated by $750 \mu\text{m}$.

Two types of film geometry were used for the resistance measurements: either the contacts were created in the top LVO film covering the whole sample surface of $5 \times 5 \text{ mm}^2$ and therefore contacting the SVO buried layer of the same surface, or the top LVO and the SVO layer were patterned in bars of a surface of $1 \times 4 \text{ mm}^2$, while the bottom LVO layer was not patterned. In this geometry, the width of the SVO layer is therefore reduced in respect to the first geometry. The resistivity was measured for both geometries. One typical problem of the measurements of the thin film resistivity using electrodes which are narrower than the thin film surface is the difficulty to determine the charge carrying width, as oxides are rather bad conductors. This charge carrying region can range from the width of the contacts to the width of the whole film. By comparison of the resistance values obtained for the two geometries with a different width of the SVO layer, the observed increase of the resistance in the second geometry shows that the charge is carried in the SVO layer, and the difference is used to calculate a reliable resistivity value. Furthermore, by this procedure, a possible conduction by an oxygen-depleted STO surface can be ruled out: In such a case, no change of the charge carrying width and therefore of the resistance value between the two geometries would be expected.

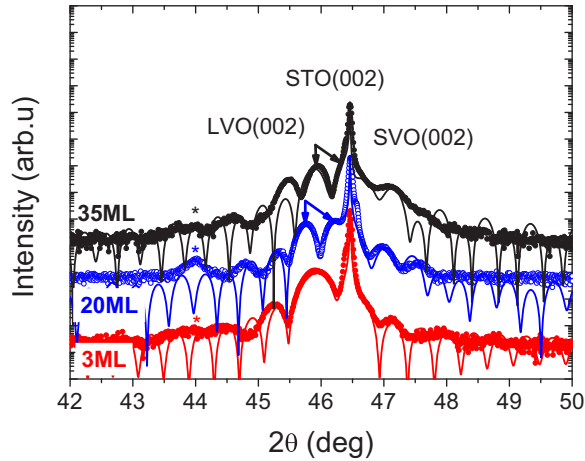


FIG. 1. (Color online) XRD scans of the (002) reflection for the samples 1 (35 ML buried SVO layer), 2 (20 ML), and 3 (3 ML). The solid arrows point to the positions of Bragg peaks of capping and bottom LVO layers, respectively; the peak at 44° marked by the star is due to the sample holder. The symbols represent the experimental data; the lines are the simulation results by coherent scattering theory.

III. RESULTS AND DISCUSSION

A. Structural characterization

Figure 1 shows the XRD scans of the (002) reflections for samples 1, 2, and 3 with decreasing thickness of SVO. The identification of the nature of the different peaks is difficult due to the presence of Laue fringes, indicating at the same time a high structural quality of the films. Therefore, the diffraction data was simulated by the coherent addition of the scattering contributions of all three layers including the truncation rod of the substrate in order to extract the thickness of the SVO layer and the out-of-plane lattice parameters of all layers. In these simulations, the structure of LVO was represented by its pseudocubic description for simplicity, although an orthorhombic description would be more correct due to the possible presence of octahedral rotations [20,23]. From these simulations, the Bragg peaks of the two LVO layers could be identified, as well as the thickness of the SVO layer at least for the two thicker films, samples 1 and 2. In sample 3, the diffraction data shows *a priori* only one Bragg peak related to LVO with an increased peak width compared to the two other samples, which could be interpreted as one LVO layer with a reduced thickness. However, sample 3 contains two LVO layers of a comparable thickness, which was confirmed by secondary ion mass spectroscopy (SIMS) during the ion beam etching of this sample. Therefore, the diffraction data was simulated with two LVO Bragg peaks with nearly the same lattice parameter, leading to a reasonable agreement in the simulation (see Fig. 1).

With the help of these simulations, the thickness of the SVO layer was extracted to be 13.5 nm (35 ML) for sample 1 and 7.7 nm (20 ML) for sample 2. For sample 3, it was not possible to extract an exact estimation from the XRD data, as the data could be simulated with comparable quality for a thickness ranging from 3 to 5 ML. In this sample, the thickness of the buried SVO layer falls into the range where a pseudogap state was found for free surface SVO layers [8]. To be more exact

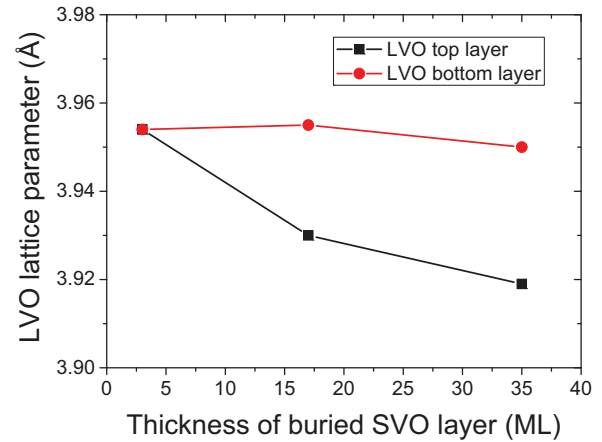


FIG. 2. (Color online) Lattice parameters of the LVO top and bottom layer versus the thickness of the buried SVO layer.

on the thickness, we used SIMS data and the growth rate of LVO and SVO estimated from different calibration processes to refine the estimation. For example, if we assume that the etching rate for SVO should stay the same for the different samples in stable etching conditions, the thickness of SVO in sample 3 can be calculated using the etching rate determined from sample 1 with a known SVO thickness. The combination of these techniques leads to a thickness of the SVO layer in sample 3 of 1.1(1) nm, which is approximately equivalent to 3 ML. So the thickness of the buried SVO layer in sample 3 is comparable to the thickness where an insulating state was found in free surface SVO films [8].

The out-of-plane lattice constant of SVO (c_{SVO}) was found to be 3.87 Å both in sample 1 and sample 2, independently of its film thickness and similar to the bulk value; due to the absence of the Bragg peak of SVO in sample 3, the lattice parameter was not extracted from the XRD data. For the LVO layers, only one of the Bragg peaks indicates a lattice parameter (c_{LVO1}) independent of the SVO layer thickness, while the other one (c_{LVO2}) shows a distinct dependence on the SVO layer thickness (see Fig. 2). As the bottom LVO layer is grown on the STO substrate, while the top LVO layer is grown on a SVO film with varying thickness, it was deduced that the LVO layer with the constant lattice parameter is the bottom one and the lattice parameter of the top LVO layer is expected to change with the thickness of the SVO layer. c_{LVO1} is found to be around 3.95 Å, comparable to single thick films of LVO [23,24] or in superlattices [25,26] with thin SVO layer. c_{LVO2} , on the other hand, varies with the thickness of the SVO film, being 3.92 Å in sample 1, 3.93 Å in sample 2, and 3.95 Å in sample 3. Thus, for 3 ML of SVO the strain state of the top LVO layer is not influenced by the intergrowth of the SVO layer, probably due to the small thickness of the latter. For thicker SVO layers, c_{LVO2} decreases, which is somewhat counterintuitive, as SVO has a smaller lattice parameter than LVO and STO. With an elastic model, an increase of c_{LVO2} would be expected. However, a decrease of the volume of the LVO unit cell with an increasing SVO thickness was also observed in the form of superlattices [27], which was attributed to a complex interplay between the elastic distortion and the change of octahedral rotations in this material under epitaxial strain.

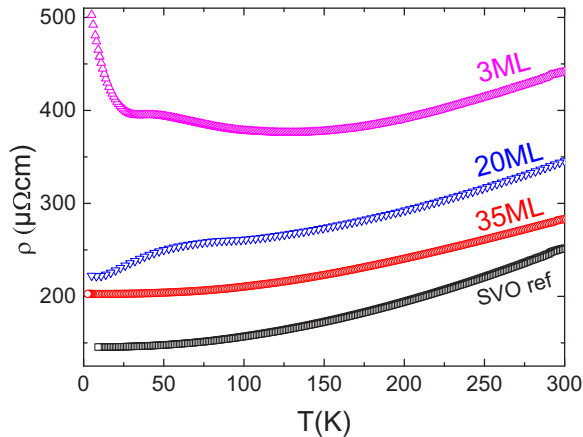


FIG. 3. (Color online) Resistivity versus the temperature for the SVO reference sample, samples 1, 2, and 3 (from bottom to top).

B. Transport properties

The resistivity ρ versus the temperature for samples 1, 2, and 3 and a thick SVO single layer sample as reference is shown in Fig. 3. In overview, all samples show metallic behavior above 100 K, indicated by the negative slope of resistivity versus temperature. Thus, even for the ultrathin layer in sample 3, the metallic phase is present. It is worth noting that the resistivity value of sample 3 (3 ML) at room temperature is only a factor of 2 higher than the reference sample, therefore the reduction of thickness does not influence essentially the conducting properties at room temperature.

In order to study the detailed transport behavior, a single layer SVO sample with the thickness of 43.5 nm has been studied as a reference. As shown in Fig. 3, the evolution of resistivity as a function of temperature shows a metallic behavior all over the measured range, while the resistivity value drops between 300 and 10 K by about a factor of 2. In general, a quadratic dependence on temperature can be observed all over the measurement range, so the data was fitted with $\rho = \rho_0 + AT^2$. The residual resistivity ρ_0 is calculated to be $145.162(48) \mu\Omega \text{ cm}$ and $A_{\text{Ref}} = 1.210(1) \text{ n}\Omega \text{ cm K}^{-2}$. The coefficient A , which quantitatively represents the electron-electron interactions in a strongly correlated system, is quite similar to the value reported by Onoda *et al.* [19] for SVO ceramics. The same authors propose also a temperature power index $n = 1.8$ for a certain temperature range, which was also possible to fit to this data (not shown here). However, the fitting parameters change only slightly compared to the T^2 fits over the complete temperature range, and no essential impact on the results of this study was observed. The residual resistivity of the single layer SVO sample is about two orders higher than the one obtained in powder samples, but it should be noted that ρ_0 is governed by the mean free time between collisions (τ), which can vary significantly due to the existence of structural defects or vacancies. By carrying out Hall measurements, the carriers were shown to be electrons and their density was extracted to be $1.9 \times 10^{23} \text{ cm}^{-3}$ with a mobility μ at 5 K around $0.2 \text{ V}^{-1} \text{ s}^{-1} \text{ cm}^2$. In the absence of SrVO₃ bulk Hall measurements in the literature, the value can be compared to La_{0.6}Sr_{0.4}VO₃ solid solutions [28], showing the same order of magnitude. A small positive magnetoresistance (MR) was

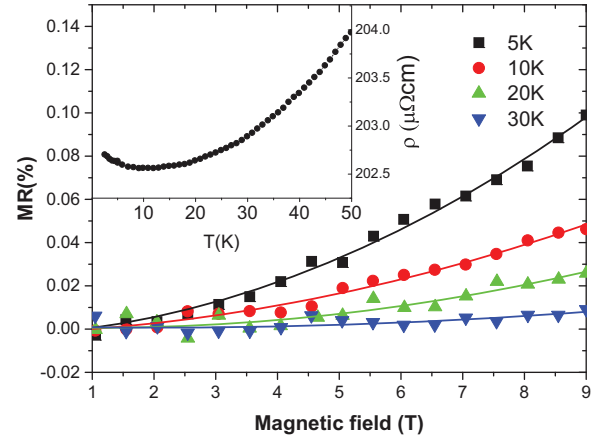


FIG. 4. (Color online) Magnetoresistance versus magnetic field for sample 1 with 13.5 nm buried SVO layer at different temperatures with H^2 fit (lines). Inset: Resistivity versus temperature in the low-temperature regime.

obtained, which is governed by the Lorentz force. However, as SVO is a correlated material, the Hall measurement results should be taken with caution. The independent quasiparticle character, which is one of the basic assumptions of the standard analysis of the Hall effect, may fail in strongly correlated systems [29–31].

Regarding the temperature dependence of the buried layers in more detail, sample 1 with 13.5-nm (35 ML) -thick SVO between the LVO layers presents a similar metallic resistivity behavior down to 10 K, compared to the single layer SVO reference sample. A T^2 dependence can be fitted from 300 to 11 K with $A_{S1} = 0.935(2) \text{ n}\Omega \text{ cm K}^{-2}$ and $\rho_0 = 201.953(75) \mu\Omega \text{ cm}$. This residual resistivity is larger than the one in the SVO reference sample due to structural defects in the buried SVO layer, and therefore a decrease of τ . This is also observed in the ratio of the resistivity at 300 and 10 K of 1.42, smaller than that of the reference sample. A_{S1} is similar to A_{Ref} , thus the electron-electron correlation in these two systems is comparable. Interesting low-temperature dependence is observed from 10 to 2 K, as a negative $\delta\rho/\delta T$ is obtained (see the inset of Fig. 4). However, the fitting for this region is difficult since the measured points are limited and the variation ratio $\Delta\rho/\rho_{10 \text{ K}}$ is as small as 0.2%, so we are not able to quantitatively analyze the underlying mechanism of this upturn.

Again, a small positive MR with H^2 behavior was observed (Fig. 4). The relative increase of the resistance is usually expressed by $\Delta\rho/\rho_0 \propto (\mu H)^2$ in the case of low field region where $\mu H > 1$, with H the magnetic field strength [31,32]. This can be qualitatively understood, as between two subsequent scattering events, the Lorentz force will deflect the electrons on their route. This will increase the path covered by the charges and the probability of collisions, thus the resistance will be increased. The observed positive MR permits one to exclude weak localization due to disorder as a mechanism for the observed upturn of the resistivity in the low field range, as in this case a negative MR would be expected [33]. Weak localization due to electron-electron

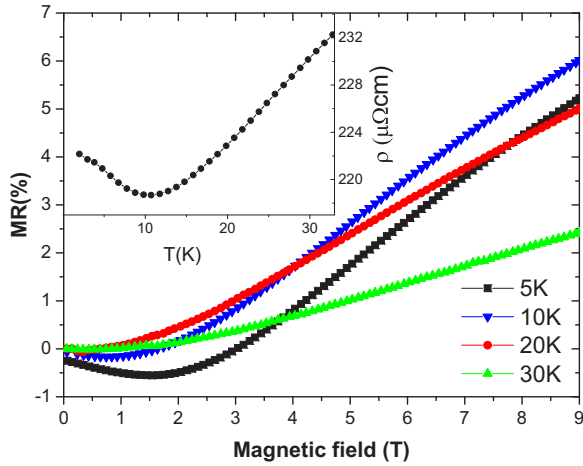


FIG. 5. (Color online) Magnetoresistance versus magnetic field for sample 2 with 7.7 nm buried SVO layer at different temperatures. Inset: Resistivity versus temperature in the low-temperature regime.

interactions remains possible, however, as a small, positive MR is compatible with the theory.

As the thickness of the buried SVO layer decreases to 7.7 nm, at high temperature the same evolution of resistivity with temperature can be observed as in sample 1 or the reference sample: A T^2 dependence with the coefficient $A_{S2} = 1.070(1) \text{ n}\Omega \text{ cm K}^{-2}$ and $\rho_0 = 249.695(51) \mu\Omega \text{ cm}$ in the temperature region from 300 to 95 K. A_{S2} is still comparable to sample 1 and the reference sample; ρ_0 is again enhanced due to the reduced thickness of the SVO layer [34]. At lower temperatures, a slight maximum in resistivity followed by a peculiar metallic phase is observed, which also appears in LVO/SVO superlattices with thin SVO [25]. Between 10 and 2 K, again, an increase of the resistivity is observed (see inset of Fig. 5), now better defined than in sample 1. The resistivity variation in this range is calculated as $(\rho_{2K} - \rho_{10K})/\rho_{10K} = 1.6$. A similar resistivity variation ratio has been recently reported in a 6.5-nm (17 ML)-thick SVO film grown on LSAT substrate by PLD with a minimum resistivity at around 50 K [10]. There, the model of VRH was applied to fit the data below 30 K. Fitting efforts of our data with the same model did not lead to satisfactory results, thus VRH does not seem to be at the origin of the observed temperature dependence in our samples.

In order to further investigate the transport properties, MR at different temperature has been measured and shown in Fig. 5. Interestingly, an important enhancement of two orders of magnitude in the MR values is observed with respect to the sample 1 and the reference sample. A strong enhancement of the MR was also found in STO/LAO heterostructures [35,36] and was ascribed to the presence of a population of high mobility electrons. The larger MR value could therefore be explained by a higher mobility of the charge carriers in sample 2 compared to sample 1. However, for a constant number of charge carriers, the enhanced mobility would also imply a lower resistivity of sample 2 compared to sample 1, which is not observed experimentally. Further investigation will be needed to well establish the origin of the rather large positive MR. Effects due to the measurement setup are excluded as

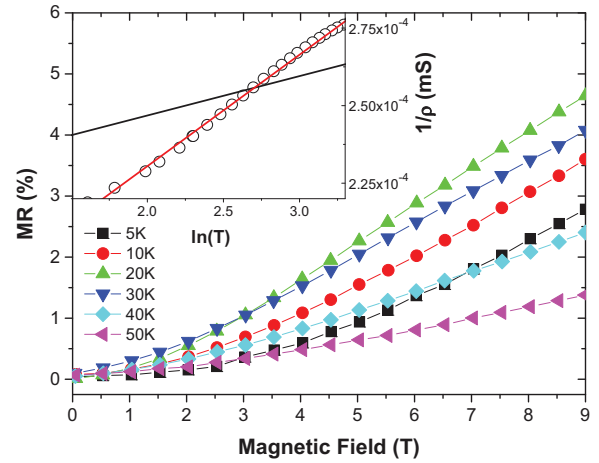


FIG. 6. (Color online) Magnetoresistance versus magnetic field for sample 3 with 1.1 nm buried SVO layer at different temperatures. Inset: Conductivity versus $\ln(T)$ in the low temperature regime. The lines are linear fits with $p = 1$ (black) and $p = 3$ (red), see text.

the reference sample and sample 1 do not show such an enhancement.

Moreover, the MR at 5 K has a complex magnetic field dependence presenting negative MR at low field and a positive one above 3 T. With the increase of temperature, the negative feature gradually vanishes and the MR turns positive also at low field above 10 K. This feature leads also to a nonmonotonous temperature dependence of the MR at 9 T (Fig. 7) indicating that the measured MR is a combination of negative and positive contributions, so that the observed field dependence may result from the superposition of the possibly different field dependencies of the two contributions. A further investigation of the field dependence below 10 K is therefore rather complicated, and will not be done here. Above 10 K, again a H^2 dependence can be identified. The negative MR contribution having vanished, the H^2 dependence may indicate again a Lorentz force related MR. The mobility of the charge carriers is the most important parameter in this theory, but as discussed before, we do not have other indications that μ is actually enhanced in sample 2.

In the 1.1-nm-thick SVO sample, a quadratic temperature dependence of the resistivity is determined down to 220 K, with the $A_{S3} = 1.020(3) \text{ n}\Omega \text{ cm K}^{-2}$ which is again comparable to the rest of the samples, indicating that charge carriers are concentrated in the SVO layer even for such a low thickness. It is worth noting that this observation is also coherent with the results of an in-depth electron microscopy study of LVO/SVO superlattice samples with 3 ML SVO layers synthesized in our group with the same equipment and growth conditions [21]. ρ_0 keeps increasing to $350.03(18) \mu\Omega \text{ cm}$. Around 100 K, a transition region is observed, with a clear increase of the resistivity below 30 K. This upturn of resistivity can be fitted by a logarithmic temperature dependence, as shown in the inset of Fig. 6. Trials to fit the data with a two-dimensional or three-dimensional VRH model failed, as also for an activated behavior.

Such a logarithmic upturn of the temperature is typically explained either by the Kondo effect [37] or by weak

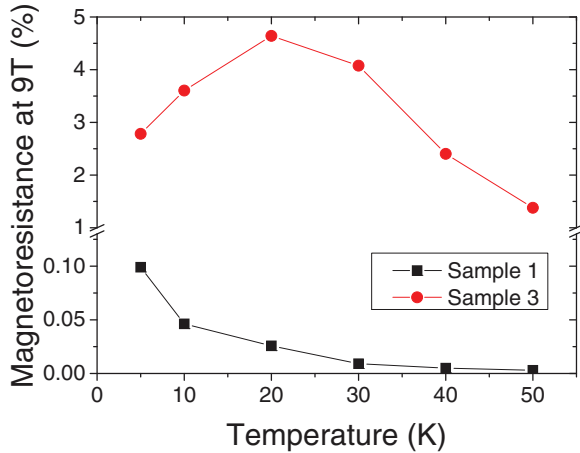


FIG. 7. (Color online) Magnetoresistance versus temperature for sample 1 (13.5 nm) and sample 3 (1.1 nm).

localization in a two-dimensional system due to coherent backscattering [1,3]. In the latter case, the corrections to the Boltzmann equation appear, when the Fermi wavelength [$\lambda_F = 2\pi/(3\pi^2 n_s)^{1/3}$] is of the same order as the mean free path ($\Lambda = \frac{h}{\rho n_s e^2 \lambda_F}$, where h is the Planck constant and e is the electron charge). For sample 3, these values are calculated from Hall effect measurements to be 2.03 and 2.52 nm, respectively. Therefore, quantum corrections should be taken into account. The difference between the two mechanisms of the resistivity upturn can be made by the sign of the MR. Both for the Kondo effect and the weak localization due to disorder, a negative MR is expected, as the magnetic field suppresses sources of scattering. This is not the case for weak localization due to electron-electron interactions [33], as here the magnetic field enhances the number of scattering events due to the longer electronic path. The MR of sample 3 (see Fig. 6) is positive over the measured magnetic field range with values in the same order of magnitude as in sample 2 (see Fig. 5), but the temperature dependence of the MR at 9 T (Fig. 7) shows a nonmonotonous dependence, indicating that also in this sample, a negative contribution to the MR is present. Thus, again, we cannot easily interpret the field dependence of the MR as the observed one is a superposition of the field dependence of both the negative and the positive contribution. Unlike the MR measured for sample 2, even at high field the data does not scale with the previously established H^2 behavior, although the observed values are in the same order of magnitude. While the 5 K MR shows this square field dependence, at higher temperature the field power decreases reaching 1.3 for 30 K.

Angular-dependent magnetoresistance measurements have been carried out in order to investigate the shape of the Fermi surface for the sample with the thinnest buried SVO layer. For a 2D transport regime, the magnetotransport will only respond to the perpendicular component of the magnetic field $B \cos(\theta)$, where θ is the angle between the applied magnetic field and the sample plane. The MR in the parallel magnetic field is negligible compared to the one with perpendicular magnetic field, indicating an anisotropic Fermi surface of the electronic structure of sample 3. In Fig. 8 we show the MR as a function

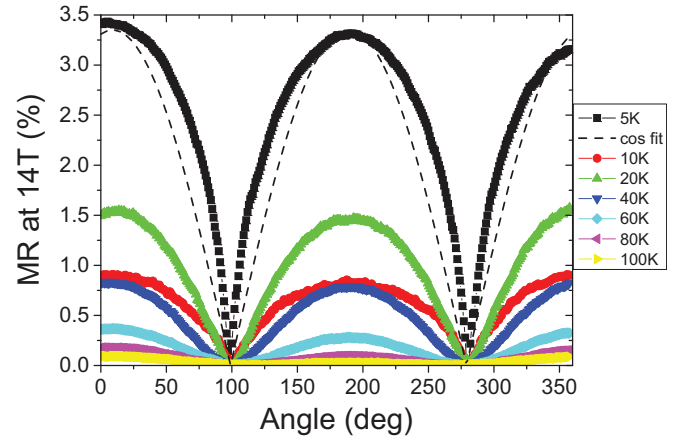


FIG. 8. (Color online) Magnetoresistance of sample 3 at 14 T versus tilt angle from 5 to 100 K. The $\cos(\theta)$ fitting and the experimental data at 5 K give a reasonable agreement.

of rotation angle while the sample was rotated in a 14 T magnetic field at different temperatures. The experimental data at 5 K can be reasonably reproduced by a cosine function. This indicates that sample 3 is only responsive to the perpendicular contribution of \mathbf{B} at an assigned angle, and thus shows 2D transport characteristics. Figure 8 also shows the MR versus the rotation angle from 5 to 100 K; the $|\cos(\theta)|$ -like behavior is maintained until 100 K, where the transition of $R(T)$ occurs.

The observation of a bidimensional character of the charge carriers allows one to interpret the logarithmic temperature dependence of the resistivity. In the case of a bidimensional, weakly localized system, the temperature dependence of the conductivity is described as follows [1]:

$$\sigma_{2D}(T) = \sigma_0 + \frac{p}{2} \frac{e^2}{\hbar\pi^2} \ln\left(\frac{T}{T_0}\right), \quad (1)$$

where σ and σ_0 are the temperature-dependent and the residual conductivity, respectively; e is the electronic charge and \hbar is the Planck's constant. p is the parameter of interest: In the case of scattering due to electron-phonon processes, p is equal to 3, while in the case of scattering due to electron-electron interactions, this parameter takes the value of 1. We have fitted the logarithmic upturn of the resistivity of sample 3 with this formalism, and the fit is shown in the inset of Fig. 6. The data follows clearly the theory with $p = 3$, so probably the scattering processes leading to the upturn of the resistivity upturn are rather due to electron-phonon scattering. Anyway, the good correspondence between the theory and the experimental data confirms the bidimensional character of the charge carriers.

The detailed analysis of the transport properties of the samples shows thus the influence of the thickness of the buried SVO layer: The 13.5-nm (35 ML)-thick film shows a behavior comparable to bulk SVO with a similar conduction and scattering. For the 7.7-nm (20 ML)-thick SVO layers, a change in the transport behavior becomes visible by the modification of the low-temperature metallic phase, and the observation of an enhanced MR of around two magnitudes higher than in the reference sample. In sample 3 with a 3 ML buried SVO layer, a clear upturn with logarithmic behavior at low temperature and

the angular-dependent magnetoresistive response indicates that this behavior is attributed to weak localization in a two-dimensional system [3], which is characterized by the presence of electronic states at the Fermi energy. So, even at low but finite temperature no insulating gap is observed for buried SVO layers down to 3 ML.

C. Discussion

Although the details are not understood completely, the above presented results indicate that, as the charge carriers are well localized in the buried layers of the strongly correlated conductor SVO, they do not go through a metal-to-insulator transition when the dimensionality is reduced from three-dimensional to two-dimensional as was observed in the free surface films. Even in the thinnest buried SVO layer, the signatures of delocalized charge carriers are observed. However, the exact origin of this observation has still to be discussed.

First, the influence of the structural properties on the electronic transport behavior has to be considered. Given the sandwich structures in this study, one may argue that the strain state of the SVO layer could be responsible for the observed discrepancies between the buried and the free surface samples. The most interesting case here is sample 3 with the 3ML SVO thickness, but the SVO is extremely thin and this information cannot be accessed directly. However, the strain state of the top LVO layer can be used as an indicator for the in-plane parameter of the underlying SVO layer. It was shown that the critical thickness of LVO on STO(001) for structural relaxation is above 70 nm [23], so it can be inferred that the 25-nm-thick bottom LVO layer grows coherently strained on the STO, notably with the same in-plane lattice parameter. The analysis of the XRD data of the top LVO layer has shown that in the case of the 3-ML-thick buried SVO layer, the top LVO layer is in the same strain state as the bottom one, indicating that the buried SVO layer has the same in-plane parameter as the STO substrate. This is only true for the 3 ML buried SVO layer. For samples 1 and 2, a different strain state of the top and the bottom LVO layer was found, indicating that in these cases, the SVO layer does not have the same in-plane lattice parameter as the STO substrate.

Therefore, the strain state of the thinnest buried SVO layer should be the same as for the single layer samples on STO(001) reported by Yoshimatsu *et al.* [8]. But even if the strain state of the 3 ML SVO monolayer would be a different one, the influence of the unit cell volume and distortion on the resistive properties should be small. Sekiyama *et al.* [38] and Georges [39] reported that, based on photoemission spectroscopy results, the V-O-V distortion does not strongly impact the occupied $3d$ states in SVO, thus even for a distorted cubic structure of the buried SVO layer, the bulk occupation of the states is expected. This is confirmed by the comparison of the obtained fit parameters of the high-temperature metallic phase of the here studied samples, where the coefficient A of the T^2 term stays generally constant, also in comparison to the reference sample. The different c_{LVO} values of the top LVO layer indicate a change in the strain state of the SVO layer with increasing thickness, but the nature and the strength of the electron-electron interaction do not seem to vary strongly. Therefore, even if the SVO layer would not be strained as

observed, a possible distortion of the SVO unit cell does not influence the electronic properties of the SVO layer in a significant way.

Moreover, the similarity of the high-temperature metallic phase in the buried SVO layers and the reference SVO layer allows us to discard a possible conduction via the LVO layers as the origin of the lack of a strongly localized or pseudogap state of the buried layers. LVO is a Mott insulator that is prone to residual conductivity due to defects. It was shown by Okamoto *et al.* [40], that at the interface of a band insulator (STO) and a Mott insulator (LaTiO_3), conduction due to the overlap of the central quasiparticle peak of the Mott insulator with the unoccupied bands near the Fermi energy of the band insulator is possible. The charges spread out of the confinement regions in a region of roughly 3 ML. In the hypothetical case of a strongly localized SVO phase, such an effect may be possible and lead to the observation of a conducting phase, although the SVO layer itself is insulating. However, in this case, the charge carriers would be localized in the LVO layer, which should change rather strongly the characteristics of the metallic phase. For example, the solid solution of $(\text{La,Sr})\text{VO}_3$, which would be a comparable system to carrier doped LVO, shows a $T^{1.5}$ dependence of the resistivity in the metallic part of the phase diagram [41], clearly different from the observed T^2 behavior in our samples.

Based on the investigated samples, an insulating state at even lower thickness of the buried SVO layer cannot be excluded, and seems even to be probable. Unfortunately, with our growth and characterization techniques we are not able to investigate thoroughly the 1 ML limit, but the weakly localized regime observed in the 3-ML-thick buried SVO layer may suggest a strongly localized state at even lower thicknesses. In order to answer the question proposed in the Introduction on the governing physics in this system, the role of the correlations in the localized state has to be highlighted. For Mott transitions, the behavior of the system approaching the MIT from the metallic state is typically characterized by an enhancement of the correlations, as shown in the $(\text{La,Sr})\text{VO}_3$ system [42]. A good indicator of the strength of the correlations is the coefficient of the temperature-dependent part of the resistivity A which, in the cited study, is enhanced by one order of magnitude while approaching the Mott transition. The coefficients of the T^2 resistivity dependence observed in the above data on the SVO buried layers stay constant [$A_{\text{ref}} = 1.210(1) \text{ n}\Omega \text{ cm K}^{-2}$, $A_{S1} = 0.935(2) \text{ n}\Omega \text{ cm K}^{-2}$, $A_{S2} = 1.070(1) \text{ n}\Omega \text{ cm K}^{-2}$, and $A_{S3} = 1.020(3) \text{ n}\Omega \text{ cm K}^{-2}$], and do not increase in a similar way. Thus, the system does not approach a Mott transition. The observed weakly localized regime seems therefore to be induced by the disorder in the system, as also indicated by the p coefficient of the logarithmic upturn. Recently, a coefficient of $p = 1$ was observed in buried SVO layers with an even higher structural quality [43], indicating that a pure 2D electron liquid state can be reached in this system, where the disorder plays a smaller role than in our samples.

Our data therefore suggests that buried 2D systems of strongly correlated oxide conductors do not unavoidably lead to a Mott insulating state, but that a state similar to a 2D electron liquid can be reached. These findings open up the way for the investigation of such 2D electron liquid materials, allowing the experimental investigation of the influence of

strong electronic correlations on the 2DEG state, and the development of gate-voltage controllable and spin sensitive channel materials for field effect transistors.

As to the possible origin of the difference in properties between buried and free surface SrVO₃, the occupancy of the different t_{2g} orbitals could play a role. It was shown in cobaltites [44] and manganites [45,46], that the orbital occupancy between the different e_g and t_{2g} orbitals can be tuned by strain or by capping layers. Such studies were not conducted on vanadates up to now, but it is possible that the orbital occupancy changes between the free surface thin films of SrVO₃ and the buried ones in this study similar to what happens in the cited systems. A study of the band structure of LaVO₃/SrVO₃ superlattices indicate local structural changes at the interface of LaVO₃ and SrVO₃ [47], which may be at the origin of a change of orbital occupation and therefore a difference in the transport properties.

IV. CONCLUSIONS

The resistive properties of buried SVO layers with a thickness down to 1 nm (3 ML) were studied. Even the

thinnest buried layer shows a metallic behavior, entering a weakly localized regime only at low temperature. An anisotropic Fermi surface and a disorder induced logarithmic temperature dependence of the resistivity indicate a true bidimensional electron liquid state. Thus, the Mott transition can be avoided in buried two-dimensional strongly correlated oxide conductors, showing up a way to develop and investigate bidimensional electronic systems with the unique features of oxide conductors.

ACKNOWLEDGMENTS

This work is financially supported by Conseil Régional de Basse Normandie, France and also guided in the framework of the Erasmus-Mundus International Doctoral School in Functional Materials (IDS FunMat). The authors want to thank A. Pautrat for technical assistance with the MR measurements. Q.L. appreciates the fruitful discussions with O. Copie, A. David, R. Frésard, K. Kolincio, H. Rotella, F. Veillon at the CRISMAT, France, and S-Y.Li and A. Klein of Institut für Materialwissenschaft, Technische Universität Darmstadt, Germany.

-
- [1] P. A. Lee and T. V. Ramakrishnan, Disordered electronic systems, *Rev. Mod. Phys.* **57**, 287 (1985).
- [2] A. J. Peter, Mott constant in two-dimensional metal-insulator transition, *Physica E* **25**, 99 (2004).
- [3] P. Wölfle and D. Vollhardt, Self-consistent theory of Anderson localization: General formalism and applications, *Int. J. Mod. Phys. B* **24**, 1526 (2010).
- [4] E. Abrahams, S. V. Kravchenko, and M. P. Sarachik, Metallic behavior and related phenomena in two dimensions, *Rev. Mod. Phys.* **73**, 251 (2001).
- [5] M. Bowen, M. Bibes, A. Barthélémy, J.-P. Contour, A. Anane, Y. Lemaître, and A. Fert, Nearly total spin polarization in La_{2/3}Sr_{1/3}MnO₃ from tunneling experiments, *Appl. Phys. Lett.* **82**, 233 (2003).
- [6] V. Pardo and W. Pickett, Electron confinement, orbital ordering, and orbital moments in d^0 - d^1 oxide heterostructures, *Phys. Rev. B* **81**, 245117 (2010).
- [7] R. von Helmolt, J. Wecker, B. Holzapfel, L. Schultz, and K. Samwer, Giant negative magnetoresistance in perovskitelike La_{2/3}Ba_{1/3}MnO_x ferromagnetic films, *Phys. Rev. Lett.* **71**, 2331 (1993).
- [8] K. Yoshimatsu, T. Okabe, H. Kumigashira, S. Okamoto, S. Aizaki, A. Fujimori, and M. Oshima, Dimensional-Crossover-Driven Metal-Insulator Transition in SrVO₃ Ultrathin Films, *Phys. Rev. Lett.* **104**, 147601 (2010).
- [9] K. Yoshimatsu, K. Horiba, H. Kumigashira, T. Yoshida, A. Fujimori, and M. Oshima, Metallic Quantum Well States in Artificial Structures of Strongly Correlated Oxide, *Science* **333**, 319 (2011).
- [10] M. Gu, S. A. Wolf, and J. Lu, Two-dimensional mott insulators in SrVO₃ ultrathin films, *Adv. Mater. Interfaces* **1**, 1300126 (2014).
- [11] R. Scherwitzl, S. Gariglio, M. Gabay, P. Zubko, M. Gibert, and J.-M. Triscone, Metal-insulator transition in ultrathin LaNiO₃ Films, *Phys. Rev. Lett.* **106**, 246403 (2011).
- [12] M. Kobayashi, K. Tanaka, A. Fujimori, S. Ray, and D. Sarma, Critical test for Altshuler-Aronov theory: Evolution of the density of states singularity in double perovskite Sr₂FeMoO₆ with controlled disorder, *Phys. Rev. Lett.* **98**, 246401 (2007).
- [13] R. Sánchez, M. Causa, A. Caneiro, A. Butera, M. Vallet-Regí, M. Sayagués, J. González-Calbet, F. García-Sanz, and J. Rivas, Metal-insulator transition in oxygen-deficient LaNiO_{3-x} perovskites, *Phys. Rev. B* **54**, 16574 (1996).
- [14] M. Kim, C. Bell, Y. Kozuka, M. Kurita, Y. Hikita, and H. Hwang, Fermi surface and superconductivity in low-density high-mobility δ -doped SrTiO₃, *Phys. Rev. Lett.* **107**, 106801 (2011).
- [15] J. Mannhart and D. G. Schlom, Oxide interfaces—An opportunity for electronics, *Science* **327**, 1607 (2010).
- [16] H. W. Jang, D. A. Felker, C. W. Bark, Y. Wang, M. K. Niranjan, C. T. Nelson, Y. Zhang, D. Su, C. M. Folkman, S. H. Baek, S. Lee, K. Janicka, Y. Zhu, X. Q. Pan, D. D. Fong, E. Y. Tsybal, M. S. Rzechowski, and C. B. Eom, Metallic and insulating oxide interfaces controlled by electronic correlations, *Science* **331**, 886 (2011).
- [17] A. Ohtomo, D. Muller, J. Grazul, and H. Hwang, Artificial charge-modulation in atomic-scale perovskite titanate superlattices, *Nature (London)* **419**, 378 (2002).
- [18] Y. Hotta, T. Susaki, and H. Hwang, Polar discontinuity doping of the LaVO₃/SrTiO₃ interface, *Phys. Rev. Lett.* **99**, 236805 (2007).
- [19] M. Onoda and H. Nagasawa, Magnetic and structural aspects of semiconducting perovskites RVO₃, *Solid State Commun.* **99**, 487 (1996).
- [20] P. Boullay, A. David, W. Sheets, U. Lüders, W. Prellier, H. Tan, J. Verbeeck, G. Van Tendeloo, C. Gatel, G. Vincze, and Z. Radi, Microstructure and interface studies of LaVO₃/SrVO₃ superlattices, *Phys. Rev. B* **83**, 125403 (2011).
- [21] H. Tan, R. Egoavil, A. Béch e, G. T. Martinez, S. Van Aert, J. Verbeeck, G. Van Tendeloo, H. Rotella, P. Boullay, A. Pautrat,

- and W. Prellier, Mapping electronic reconstruction at the metal-insulator interface in $\text{LaVO}_3/\text{SrVO}_3$ heterostructures, *Phys. Rev. B* **88**, 155123 (2013).
- [22] W. Meevasana, P. D. C. King, R. H. He, S.-K. Mo, M. Hashimoto, A. Tamai, P. Songsirithigul, F. Baumberger, and Z.-X. Shen, Creation and control of a two-dimensional electron liquid at the bare SrTiO_3 surface, *Nat. Mater.* **10**, 114 (2011).
- [23] H. Rotella, U. Lüders, P.-E. Janolin, V. Dao, D. Chateigner, R. Feyerherm, E. Dudzik, and W. Prellier, Octahedral tilting in strained LaVO_3 thin films, *Phys. Rev. B* **85**, 184101 (2012).
- [24] Y. Hotta, Y. Mukunoki, T. Susaki, H. Y. Hwang, L. Fitting, and D. A. Muller, Growth and epitaxial structure of LaVO_x films, *Appl. Phys. Lett.* **89**, 031918 (2006).
- [25] A. David, R. Frésard, P. Boullay, W. Prellier, U. Lüders, and P.-E. Janolin, Structural transition in $\text{LaVO}_3/\text{SrVO}_3$ superlattices and its influence on transport properties, *Appl. Phys. Lett.* **98**, 212106 (2011).
- [26] W. Sheets, P. Boullay, U. Lüders, B. Mercey, and W. Prellier, Artificial charge modulation in perovskite vanadate superlattices, *Thin Solid Films* **517**, 5130 (2009).
- [27] U. Lüders, Q.-R. Li, R. Feyerherm, and E. Dudzik, The evolution of octahedral rotations of orthorhombic LaVO_3 in superlattices with cubic SrVO_3 , *J. Phys. Chem. Solids* **75**, 1354 (2014).
- [28] E. Prasad, M. Sayer, and J. Noad, Anderson localization and electrical $\frac{1}{f}$ noise in lanthanum strontium vanadate, *Phys. Rev. B* **19**, 5144 (1979).
- [29] P. Prelovsek, Hall effect of charge carriers in a correlated system, *Phys. Rev. B* **55**, 9219 (1997).
- [30] H. Eng, P. Limelette, W. Prellier, C. Simon, and R. Frésard, Unconventional Hall effect in oriented $\text{Ca}_3\text{Co}_4\text{O}_9$ thin films, *Phys. Rev. B* **73**, 033403 (2006).
- [31] G. Pearson and H. Suhl, The Magneto-Resistance Effect in Oriented Single Crystals of Germanium, *Phys. Rev.* **83**, 768 (1951).
- [32] I. Žutić, J. Fabian, and S. Das Sarma, Spintronics: Fundamentals and applications, *Rev. Mod. Phys.* **76**, 323 (2004).
- [33] B. Altshuler, A. Aronov, and P. Lee, Interaction effects in disordered fermi systems in two dimensions, *Phys. Rev. Lett.* **44**, 1288 (1980).
- [34] T. Coutts, Electrical conduction in thin continuous films, *Thin Solid Films* **7**, 77 (1971).
- [35] A. Joshua, S. Pecker, J. Ruhman, E. Altman, and S. Ilani, A universal critical density underlying the physics of electrons at the $\text{LaAlO}_3/\text{SrTiO}_3$ interface, *Nat. Commun.* **3**, 1129 (2012).
- [36] E. Flekser, M. Ben Shalom, M. Kim, C. Bell, Y. Hikita, H. Y. Hwang, and Y. Dagan, Magnetotransport effects in polar versus non-polar SrTiO_3 based heterostructures, *Phys. Rev. B* **86**, 121104 (2012).
- [37] J. Kondo, Resistance minimum in dilute magnetic alloys, *Prog. Theor. Phys.* **32**, 37 (1964).
- [38] A. Sekiyama, H. Fujiwara, S. Imada, S. Suga, H. Eisaki, S. I. Uchida, K. Takegahara, H. Harima, Y. Saitoh, I. A. Nekrasov, G. Keller, D. E. Kondakov, A. V. Kozhevnikov, T. Pruschke, K. Held, D. Vollhardt, and V. I. Anisimov, Mutual Experimental and Theoretical Validation of Bulk Photoemission Spectra of $\text{Sr}_{1-x}\text{Ca}_x\text{VO}_3$, *Phys. Rev. Lett.* **93**, 156402 (2004).
- [39] A. Georges, Strongly correlated electron materials: Dynamical mean-field theory and electronic structure, in *Lectures on the Physics of Highly Correlated Electron Systems VIII: Eighth Training Course in the Physics of Correlated Electron Systems and High-Tc Superconductors*, AIP Conf. Proc. No. 715, (AIP, Melville, NY, 2004), p. 3.
- [40] S. Okamoto and A. J. Millis, Spatial inhomogeneity and strong correlation physics: A dynamical mean-field study of a model Mott-insulator–band-insulator heterostructure, *Phys. Rev. B* **70**, 241104 (2004).
- [41] S. Miyasaka, T. Okuda, and Y. Tokura, Critical behavior of metal-insulator transition in $\text{La}_{1-x}\text{Sr}_x\text{VO}_3$, *Phys. Rev. Lett.* **85**, 5388 (2000).
- [42] F. Inaba, T. Arima, T. Ishikawa, T. Katsufuji, and Y. Tokura, Change of electronic properties on the doping-induced insulator-metal transition in $\text{La}_{1-x}\text{Sr}_x\text{VO}_3$, *Phys. Rev. B* **52**, R2221 (1995).
- [43] A. Fouchet (private communication).
- [44] D. W. Jeong, W. S. Choi, S. Okamoto, J.-Y. Kim, K. W. Kim, S. J. Moon, D.-Y. Cho, H. N. Lee, and T. W. Noh, Dimensionality control of d-orbital occupation in oxide superlattices, *Sci. Rep.* **4**, 6124 (2014).
- [45] D. Pesquera, G. Herranz, A. Barla, E. Pellegrin, F. Bondino, E. Magnano, F. Sánchez, and J. Fontcuberta, Surface symmetry-breaking and strain effects on orbital occupancy in transition metal perovskite epitaxial films, *Nat. Commun.* **3**, 1189 (2012).
- [46] S. Valencia, L. Peña, Z. Konstantinovic, L. Balcells, R. Galceran, D. Schmitz, F. Sandiumenge, M. Casanove, and B. Martínez, Intrinsic antiferromagnetic/insulating phase at manganite surfaces and interfaces, *J. Phys.: Condens. Matter* **26**, 166001 (2014).
- [47] C. Schuster, U. Lüders, R. Frésard, and U. Schwingenschlögl, Lattice relaxation and ferromagnetic character of $(\text{LaVO}_3)_m/\text{SrVO}_3$, *Europhys. Lett.* **103**, 37003 (2013).